

# Electrospun polyamide thin film composite forward osmosis membrane: Influencing factors affecting structural parameter

Leila Ghadiri<sup>1</sup>, Ali Bozorg<sup>\*2</sup> and Alireza Shakeri<sup>1</sup>

<sup>1</sup>School of Chemistry, College of Science, University of Tehran, P.O. Box 14155-6619, Tehran, Iran

<sup>2</sup>Department of Biotechnology, College of Science, University of Tehran, P.O. Box: 14176-14411 Tehran, Iran

(Received September 22, 2018, Revised October 29, 2018, Accepted August 16, 2019)

**Abstract.** Poly Sulfone nanofibers were electrospun to fabricate membranes of different characteristics. To fabricate the fiber mats, polymer concentration, flowrate, and current density were determined as the most influencing factors affecting the overall performance of the membranes and studied through Response Surface Methodology. The Box-Behnken Design method (three factors at three levels) was used to design, analyze, and optimize the parameters to achieve the best possible performance of the electrospun membranes in forward osmosis process. Also, internal concentration polarization that characterizes the efficiency of the forward osmosis membranes was determined to better assess the overall performance of the fabricated electrospun membranes. Water flux to reverse salt flux was considered as the main response to assess the performance of the membranes. As confirmed experimentally, best membrane performance with the minimal structural parameter value could be achieved when predicted optimal values were used to fabricate the membranes through electrospinning process.

**Keywords:** forward osmosis; electrospinning; optimization; structural parameter; design of experiment; response surface methodology

## 1. Introduction

Potable water shortage is one of the most serious environmental crises threatening not only human sustainable existence and development, but also endangered the very existence of all life forms on the planet (Shannon *et al.* 2008). Studies have shown that more than 1.2 billion people on earth currently lack access to safe drinking water. It has also been reported that, as 2.6 billion people have little or no sanitation for their drinking water, millions of people die each year from water related infectious diseases (Montgomery and Elimelech 2007). Membrane-based separation technologies in which clean water can be produced through desalination of ubiquitous saline seawater are perhaps the best solution to address the ever-increasing water scarcity around the world (Werber *et al.* 2016).

Since the development of membrane-based desalination technologies, pressure driven processes such as microfiltration (MF), ultrafiltration (UF), nanofiltration (NF), and reverse osmosis (RO) have gained more interests over the last decades. However, although have been successfully used in practice, high energy consumption besides the quick formation and compaction of fouling layer have restricted industrial application of such processes (She *et al.* 2016). In contrast, osmotically driven membrane processes including forward osmosis (FO) and pressure retarded osmosis (PRO) processes rely on transmembrane osmotic pressure difference, naturally created by a more

concentrated draw solution (DS) (McCutcheon and Elimelech 2008, Xu *et al.* 2010). Accordingly, not only minimal fouling propensities, but also lower energy consumption would also be expected in such processes, making them promising alternatives in a variety of applications including water purification, agricultural irrigation, food processing, and power generation (Klaysom *et al.* 2013, Liu *et al.* 2015, Sudeeptha *et al.* 2017). However, although owing to their many advantages, FO has recently gained growing interest and found wide applications in water desalination, such processes suffer from some disadvantages such as water recovery, draw solution recovery cost, and internal concentration polarization (ICP). Also, it should be noted that, due to their large size and suspension state in water (Ge *et al.* 2013), not all draw solutions perform as effective as the inorganic salt solutions, and thereby, there are also some problems in finding appropriate draw solution to achieve advanced FO performance. Furthermore, problems associated to all membrane processes such as clogging and bioclogging in the presence of microorganisms, process scaling should also be considered in FO processes and practical solutions to overcome such issues should be developed (Lutchmiah *et al.* 2014).

In FO processes, with sufficient mechanical stability, commercial thin-film composite (TFC) membranes have demonstrated excellent water permeability, appropriate salt rejection, and high chemical stability. A TFC membrane typically consists of a thin rejection active layer on top of a thick porous substrate (support layer) (Tiraferrri *et al.* 2011, Wang *et al.* 2010).

Despite technical progresses, FO still suffers from ICP that takes place within the porous support layer (Li *et al.*

\*Corresponding author, Associate Professor  
E-mail: [abozorg@ut.ac.ir](mailto:abozorg@ut.ac.ir)

2011). Depends on the orientation of the asymmetric FO membrane, two distinct types of ICP effect would be expected. When the active layer of the membrane is facing the draw solution (PRO mode), solutes of the feed solution (FS) carried by the convective water flow penetrate into the open pores of the support layer. However, the active layer prevents further permeation of solutes and does not let them pass through the membrane to the DS side. This implies that the solute concentrations within the support layer would be increased (denoted as concentrative ICP) (Li *et al.* 2011, McCutcheon and Elimelech 2006). In contrast, when the active layer is in contact with the FS (FO mode), as nothing but the water can pass through the active layer, the permeated water lowers the concentration gradient across the support layer (denoted as dilutive ICP) (Loeb *et al.* 1997). To better understand the ICP effect, structural parameter ( $S$ ) has been introduced as a function of support layer characteristics as following (Wong *et al.* 2012)

$$S = \frac{\tau \times t}{\varepsilon} \quad (1)$$

where  $\varepsilon$  is porosity,  $\tau$  is tortuosity, and  $t$  is the thickness of the support layer. An ideal FO membrane of minimal ICP should possess minimal  $S$  value (Alsvik and Hägg 2013). This implies that a very thin and porous support layer with minimal tortuosity would be required to achieve the best possible performance of an FO membrane (Liu *et al.* 2016). Therefore, besides the nature of the polymer that the support layer is made of, the fabrication technique also plays a critical role in ultimate performance of the FO membrane (Song *et al.* 2011). Support layers are commonly prepared through casting technique followed by phase inversion process. Interfacial polymerization (IP) would be then conducted between two reactive monomers to form polyamide (PA) thin active layer. So far, different strategies have been introduced to control the unpleasant ICP effect in the casted film (Huang *et al.* 2013, Liu and Ng 2015, Rastgar *et al.* 2017). However, none of the proposed approaches is entirely free of scientific or practical problems and thus, to be used in large scale desalination plants, such issues should be carefully considered.

Rapidly growing electrospinning is a versatile and inexpensive method that has been used in fabrication of non-woven fibrous structures (Barhate *et al.* 2006, Borge *et al.* 2009, Yoon *et al.* 2009). Higher porosity, lower base weight, high specific area-to-volume ratio, as well as interconnected pores are the promising characteristics that electrospun membranes possess (Hoover *et al.* 2013, Wang *et al.* 2012). Using electrospinning technique, a high electric field would be applied to produce nanofibrous membranes from conventional polymers like polysulfone (PSU) or polyethersulfone (PES). The transferred electrostatic charge causes repulsive coulomb interactions in the polymer fluid, thereby characterizing the ultimate architecture of the fiber through jet instabilities (Wendorff *et al.* 2012). It has been shown that the morphology of the obtained fibrous films can be readily manipulated at nano-scale level by varying the electrospinning conditions and/or characteristics of the polymeric solution. On the other hand, we already know that in FO processes, morphology of the

support layer controls the movement of solutions accumulated within the support layer toward either the feed or draw reservoirs. Therefore, when used to fabricate the support layer, electrospinning conditions can be optimized to lower the ICP effect as the main bottleneck of the FO process, resulting in an electrospun FO membrane of high performance.

Electrospun mat was first introduced as a novel substrate of FO membrane by Bui and coworkers (Bui *et al.* 2011). Afterwards, it was reported that the scaffold-like nanofiber support layers made via electrospinning were able to successfully break the intrinsic ICP effect and it was shown that the structure parameter (Eq. 1) of commercial FO membrane could be considerably declined from 620  $\mu\text{m}$  to 80  $\mu\text{m}$ , when electrospun PES was employed as the support layer of the FO membrane. Using different combinations of polyacrylonitrile and cellulose acetate, nanofibrous substrates were fabricated via electrospinning method and their performances in terms of the water permeation and salt rejection were experimentally assessed in FO desalination systems (Bui, Nhu-ngoc and McCutcheon 2013). When compared to the standard commercial FO membranes, the novel membranes revealed improved performances with up to three times enhanced water flux and 90 % reduced salt passage. The electrospun modified membranes were also employed in PRO system to generate energy by harnessing the osmotic pressure gradient and increasing the water flux through the membrane (Bui and McCutcheon 2014).

The polymers used in the fabrication of support layer is commonly hydrophobic and their hydrophilicity can be further reduced when fibrous morphology is established via electrospinning. Many studies have been conducted to verify the influencing factors affecting the hydrophilicity of the polymers and their results have been used to manipulate the hydrophilicity of electrospun support layers (Obaid *et al.* 2016a,b, Park *et al.* 2018). However, although published studies demonstrate that the nanofibrous FO membranes can have great potential in practice, neither their desalination performance in terms of the water permeation and salt rejection, nor the parameters affecting the structure of the electrospun mat have been yet well studied. Herein, the most probable factors influencing the electrospun morphology have been systematically studied. Experiments have been conducted to determine how such influencing factors characterize the ultimate morphology of the support layer. Using Box-Behnken design (BBD), individual and interactive impacts that such independent factors could have on the structure of the electrospun support layer were assessed and used to evaluate the optimum conditions in which FO membrane support layer of highest performance and lowest structural parameter could be fabricated via electrospinning process.

## 2. Materials and methods

### 2.1 Chemicals and reagents

Polysulfone (PSU, molecular weight: 60,000, BASF Co., Germany) dissolved in N,N-dimethylformamide

(DMF, Merck) was used to fabricate the support layers. The polyamide (PA) thin layer was synthesized through interfacial polymerization of 1, 3-phenylenediamine (MPD, >99%, Merck) and 1, 3, 5-benzenetricarbonyl trichloride (TMC, >98%, Merck) monomers. TMC and MPD were dissolved in n-hexane (~99%) and distilled water, respectively. Throughout the FO experiments, solution of sodium chloride (NaCl, ≥99.8%, Iran Mineral Salts Company) and DI water were used respectively as draw and feed solutions to maintain sufficient osmotic pressure across the membrane.

## 2.2 Electrospinning parameters

Using electrospinning method, it would be possible to produce polymeric fibers from nanometers to microns in diameter based on the applied operational conditions and consequently, it is necessary to optimize the parameters regulating the electrospinning process. The practical parameters influencing the obtain electrospun structure and their values were selected based on the information published in literature (Cojocaru *et al.* 2017; Li *et al.* 2008; Pascariu *et al.* 2017). Preliminary studies were also conducted to verify such influencing parameters and assess the range in which they have highest impacts on the fabricated electrospun fibers. Such intervals were selected based on the best P-values obtained in the experiments.

## 2.3 Electrospinning polymer solutions

All polymer solutions were prepared by dissolving pre-weighed amount of PSU polymer beads in DMF. Three different polymer dope solutions with concentrations of 18, 21, and 24 wt% were prepared, degassed overnight at room temperature, and subsequently used as polymer solution in electrospinning process.

## 2.4 Preparation of PSU electrospun fiber

Using a syringe pump (5 ml), the obtained polymer solutions were pushed slowly into high voltage charged sprayer. A positive voltage of up to 30 kV was applied to the needle tip separated by 10 cm from the grounded collector. During the electrospinning process, support layers of fibrous structures were formed on an aluminum foil collector with a rotating speed of 600 rpm. Different flowrates (Table 1) were also used to inject PSU polymer solutions through the syringe pump.

## 2.5 Treatment of electrospun PSU (ESPSU)

After being peeled off the aluminum foil surface, substrates possess poor mechanical strength and would not be appropriate to be used in any desalination process. Therefore, to fuse the fibers together and provide the substrate with higher structural integrity and enhanced mechanical properties, after being fabricated, the obtained polymeric electrospun substrates were placed in an oven to keep their temperature between glass transition and melting point of PSU host polymer. The mats were placed between two pieces of glass plates and after being heated for 1 hour,

slowly cooled down to the room temperature.

## 2.6 Preparation of electrospun thin-film composite (ESTFC) membranes

Following the thermal treatment, the aqueous solution of 2 wt% MPD was poured on the PSU electrospun support layers (9.62 cm<sup>2</sup>) fixed between two clamps and the excess solution was removed via a piece of filter paper after 30 min. The obtained films were then soaked in TMC solution (0.1 wt%) for 1 min to conduct IP reaction, resulting in the formation of final polyamide dense layer (Muscatello *et al.* 2017). The prepared ESTFC membranes were finally left for 5 min at 70 °C to be dried.

## 2.7 Membrane performance assessment

The water permeability coefficient ( $K_w$ ), salt permeability coefficient ( $K_s$ ), and salt rejection rate ( $R$ ) were determined for each membrane using a dead-end RO test setup and an applied pressure of 1 bar. The effective membrane area was 9.62 cm<sup>2</sup> and the FS temperature was adjusted at 25 °C. The volume of permeate water collected within the specified time intervals was recorded to determine the permeability of the membranes. The  $R$  value was also evaluated by measuring the evolving conductivity (AD332 EC/TDS meter) of the FS initially containing 1000 ppm NaCl and the permeate solution achieved through the RO experiment. The obtained values were then used to calculate  $K_w$ ,  $K_s$ , and  $R$  as following (Salehi *et al.* 2017b)

$$K_w = \frac{J_v}{\Delta P} \quad (2)$$

$$(1 - R)/R = \frac{k_s}{k_w(\Delta P - \Delta \pi)} \quad (3)$$

$$R = 1 - \left( \frac{C_p}{C_f} \right) \quad (4)$$

Using a lab-scale cross-flow FO setup (Rastgar *et al.* 2017; Salehi *et al.* 2017a), forward osmosis performances of the membranes were investigated. At a constant cross-flow rate of 0.2 L/min (~8 m/s), both DS and FS were counter currently circulated over either sides of the FO membrane in both PRO (PA active layer facing DS) and FO (PA active layer facing FS) modes. Using a digital weight balance (EK-4100i, A & D Co, Japan) connected to a computer data logging system, the amount of permeate water collected at the DS side was exactly recorded and the FO water flux ( $J_v$ , L m<sup>-2</sup> h<sup>-1</sup>, denoted as LMH) and reverse salt flux ( $J_s$ , g m<sup>-2</sup> h<sup>-1</sup>, denoted as gMH) of the membranes were calculated as follows (Rastgar *et al.* 2018)

$$J_v = \frac{\Delta V}{A_m \Delta t} \quad (5)$$

$$J_s = \frac{(C_t V_t) - (C_0 V_0)}{A_m \Delta t} \quad (6)$$

where  $\Delta V$  (L) is the volume change of the DS over a predetermined time interval  $\Delta t$  (h). Also,  $C_0$  and  $V_0$  are the initial salt concentration and FS volume, and  $C_t$  and  $V_t$  are

their corresponding values at time  $t$ . The  $S$  value of the substrate can also be calculated by fitting the  $K_w$ ,  $K_s$ , and  $FO$  water flux values into the following equations (Liu and Ng, 2015; Loeb *et al.* 1997):

FO mode:

$$J_V = \left( \frac{1}{K_m} \right) \ln \frac{k_w \times \pi_{D,b} + k_s}{k_w \times \pi_{F,m} + J_V + k_s} \quad (FO \text{ mode}) \quad (7)$$

$$J_V = \left( \frac{1}{K_m} \right) \ln \frac{k_w \times \pi_{D,m} - J_V + k_s}{k_w \times \pi_{F,b} + k_s} \quad (PRO \text{ mode}) \quad (8)$$

where  $\pi_{D,b}$ ,  $\pi_{F,b}$ ,  $\pi_{D,m}$ , and  $\pi_{F,m}$  are respectively the osmotic pressure of the bulk DS, osmotic pressure of the bulk FS, osmotic pressure on the surface of FO membrane in DS, and osmotic pressure on the surface of FO membrane in FS. Also,  $K_m$  refers to the solute resistivity within the porous support layer which can be calculated using the solute diffusion coefficient ( $D_s$ ) and thickness ( $l$ ), tortuosity ( $\tau$ ), and porosity ( $\epsilon$ ) of the membrane support layer as following (Altaee and Sharif, 2015)

$$K_m = \frac{l\tau}{\epsilon D_s} \quad (9)$$

## 2.8 Membranes characteristics

To calculate the membrane porosity ( $\epsilon$ ), the fabricated membranes were initially weighted and then soaked in water overnight at room temperature. The weight of water saturated membranes were finally determined after removing the surface extra water to calculate the membrane porosity ( $\epsilon$ ) as following (Rastgar *et al.* 2017)

$$\epsilon = \frac{\frac{W_2 - W_1}{\rho_w}}{\frac{W_2 - W_1}{\rho_w} + \frac{W_1}{\rho_p}} \quad (10)$$

where  $\rho_w$  is density of water,  $\rho_p$  is PSU density (1.24 kg/m<sup>3</sup>) and  $W_1$  and  $W_2$  are the weights of dry and water saturated membranes, respectively. For each membrane, thickness was evaluated at three points by using a digital micrometer. Using attenuated total reflectance Fourier transform infrared (ATR-FTIR) spectroscopy, the composition and chemical bonding of the membranes were assessed. Morphological characteristics of the ESPSU support layers and ESTFC membranes from top side were qualitatively evaluated by scanning electron microscope (SEM, Zeiss, DSM 960 A, Germany). The surface hydrophilicity of ESPSU support layers and ESTFC membranes was specified by contact angle measurements by using an optical tensiometer (Dataphysics, OCA 15 plus) equipped with an image processing software.

## 2.9 Experimental design

The effect of parameters affecting the  $S$  value, including current density, flowrate, and polymer concentration were studied to assess their influences on the membranes performance expressed in terms of the  $J_v$  to  $J_s$  ratio. Box-Behnken design (Table 2) composed of 16 runs divided in

Table 1 Electrospinning process parameters with corresponding variables (coded and actual) used to fabricate different FO membranes

Design variable	Coded variable	Coded versus actual values		
		-1	0	+1
Current density Cd (KV/cm)*	C	2.0	2.5	3.0
Flowrate F (mL/hr)	B	0.7	1.0	1.3
Polymer concentration Con (wt%)	A	18	21	24

\*V/D = voltage per distance between the needle tip and collector that was constantly adjusted at 10 cm

two blocks, each with two central points, was used to conduct the experiments (Ferreira *et al.* 2007; Gönen *et al.* 2016). Considering the capability of the experimental setup and the conducted preliminary studies, the range of the operating conditions were selected (Table 1) and optimized by RSM. Experimental design, mathematical modeling, and optimization were performed using Design-Expert software (version 10.04). The obtained experimental results were analyzed by the response surface regression procedure to fit a quadratic polynomial equation using the least-square method (Kim *et al.* 2015; Nam *et al.* 2018)

$$Y = \beta_0 + \sum_{i=1}^k \beta_i x_i + \sum_{i=1}^k \beta_{ii} x_i^2 + \sum_i \sum_{i < j} \beta_{ij} x_i x_j + \epsilon \quad (11)$$

where  $Y$  is the predicted response ( $J_v/J_s$ ),  $\beta_0$ ,  $\beta_i$ ,  $\beta_{ii}$ , and  $\beta_{ij}$  are respectively the constant, linear, quadratic, and two factors interaction coefficients,  $\epsilon$  is the residual (error or noise) term, and  $X_i$  and  $X_j$  are the independent variables studied. The polynomial model was fitted to the response data obtained from the experimental design.

## 3. Results and discussion

### 3.1 Experimental

#### 3.1.1 Water flux and reverse salt flux

A laboratory-scale counter current FO system equipped with a cross-flow cell, with an effective membrane area of 9.62 cm<sup>2</sup> was used to assess water and solute fluxes across the membranes in both FO mode and PRO mode (Fig. 1). At 25 °C, FS and DS were circulated over either sides of the membranes at a fixed crossflow velocity of 8.3 m/s. Each experiment was conducted in triplicates to ensure the reproducibility of the results (Fig. 1). According to the obtained results, in the FO mode of operation, highest water flux to the reverse solute flux ratio was achieved in Run 12 (Table 2). Fig. 1 shows water fluxes ( $J_v$ ) and reverse solute fluxes ( $J_s$ ) achieved in the FO and PRO experiments conducted with 1 M NaCl and DI water as DS and FS, respectively.

Table 2 Response surface methodology (RSM) for the electrospinning process and results of BBD ( $Z_i$  denotes level of each parameter)

Run	Factors (controllable input variables)						Response (L/gr)	
	Current density		Feed flowrate		polymer concentration		(J <sub>v</sub> /J <sub>s</sub> ) – FO process	
	CD (kV/cm)	$Z_1$	F (ml/hr)	$Z_2$	Con (%)	$Z_3$	Experimental	Predicted
1	2.5	0	1.0	0	21	0	4.87907	4.80656
2	2.5	0	1.3	+1	24	+1	4.05553	3.68833
3	2.5	0	1.3	+1	18	-1	3.214715	3.27807
4	2.5	0	0.7	-1	18	-1	3.548967	3.91617
5	2.0	-1	1.0	0	24	+1	3.524206	3.83084
6	2.0	-1	0.7	-1	21	0	3.830447	3.58716
7	2.0	-1	1.3	+1	21	0	3.223359	3.28393
8	3.0	+1	1.3	+1	21	0	3.334934	3.57822
9	2.5	0	1.0	0	21	0	4.853005	4.80656
10	3.0	+1	1.0	0	18	-1	4.356373	4.04974
11	2.5	0	0.7	-1	24	+1	4.875603	4.81225
12	3.0	+1	0.7	-1	21	0	5.097593	5.03702

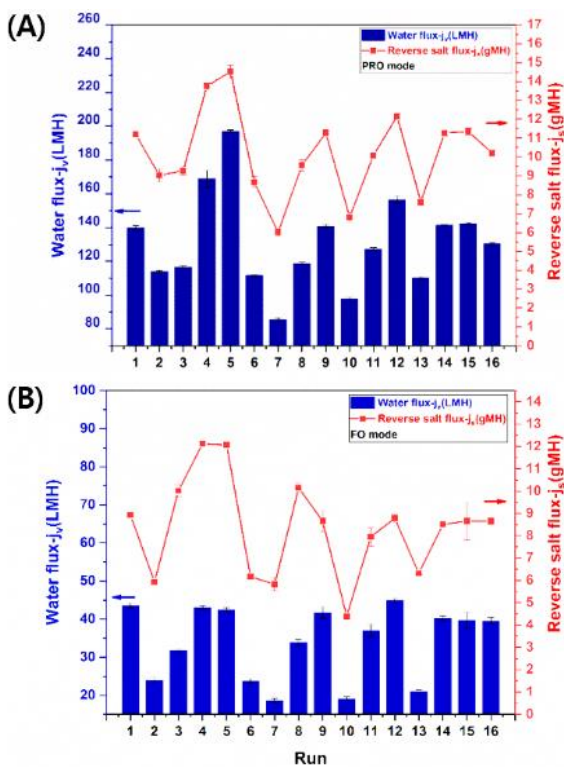


Fig. 1 Water flux (blue) and reverse salt flux (red) of the TFC membranes in (A) PRO mode and (B) FO mode of operation. Experiments were all conducted at  $25 \pm 1$  °C with 1M NaCl as DS, DI water as FS, cross-flow velocity of 8.3m/s, and membrane surface area of 9.62 cm<sup>2</sup>

### 3.1.2 ATR-FTIR

The ATR-FTIR spectrum of the obtained TFC (PSU/PA) and PSU support layer substrates are shown in Fig. 2. Following the IP reaction, new characteristic peaks at 1548 cm<sup>-1</sup> (–N–H bending vibration of amide), 1660 cm<sup>-1</sup> (–C=O stretching vibration of amide), and 1608 cm<sup>-1</sup> (aromatic ring

breathing of amide) were revealed, implying successful formation of PA active layer (Bui *et al.* 2011).

## 3.2 Statistical studies

### 3.2.1 Design of experiments analysis

The main objective of RSM is to find an appropriate model to predict and optimize the process responses. In this study, the RSM was used to determine regression model of electrospinning process to predict the structure and characteristics of the fabricated electrospun membranes. A second order polynomial regression model of three independent variables including 3 linear, 3 quadratic, and 3 interaction terms plus one block term was employed and optimized via a three level Box-Behnken experimental design. Accordingly, using a least square fit of the data provided in Table 2, following quadratic model (Eq. 12) was developed and used to verify the relationship between the response and the 3 independent variables of interest

$$\begin{aligned}
 Y = & -30.33 + 1.13Con + 7.28F + 14.99CD \\
 & + 0.18Con \times F - 0.05Con \times CD \\
 & - 1.92F \times CD - 0.02Con^2 \\
 & - 4.10F^2 - 2.26CD^2
 \end{aligned} \quad (12)$$

The effects of the independent variables and their interactions on the dependent variable were also investigated by preparing a Pareto chart. Considering the Eq. 12, the effect of each term on the model response (Fig. 3) was calculated as following (Khataee *et al.* 2010)

$$P_i = \frac{\beta_i^2}{\sum_{i=1}^n \beta_i^2} \times 100 \quad (i \neq 0) \quad (13)$$

where  $P_i$  is the percentage effect of each factor and  $\beta_s$  represent coefficients introduced in Eq. 11 and defined in Eq. 12. According to the obtained Pareto diagram (Fig. 3),

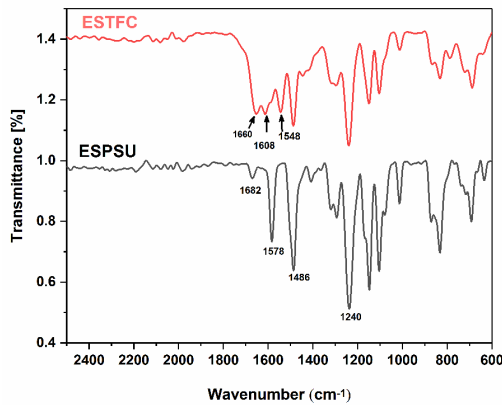


Fig. 2 Important functional groups in FTIR spectrum are  $1240\text{ cm}^{-1}$  (C–O stretch),  $1486\text{ cm}^{-1}$  (aromatic C–C),  $1578\text{ cm}^{-1}$  (C=C),  $1682\text{ cm}^{-1}$  (C=O)

Cd and F were determined as the two most influencing parameters affecting the performance of the membrane.

According to the Pareto graphic analysis, CD was found to have the highest effect on the response variable. Also, it could be concluded that all the interactive effects, except for the  $F^2$ , could be neglected based on their low  $P_i$  values. Consequently, the major influencing factors were found to be main CD (73.75%), F (17.40%), and quadratic  $F^2$  (5.62%). The experimental design and the results of the BBD conducted to verify the influence of the parameters on the fabricated ESPSU membrane have been summarized in Table 2.

As shown experimentally, the best result with the highest  $J_v/J_s$  value was achieved in RUN 12. Positive impacts of all 3 independent factors were confirmed through the obtained information (Eq. 12), meaning that, in the range of the study, the higher the polymer concentration, flowrate, and current density, the higher the ratio of water to reverse salt fluxes. Also, as confirmed by the Pareto chart (Fig. 3), among the three independent variables, current density and polymer concentration were found to have the most and the least impacts on the response variable, respectively. Furthermore, optimization of the electrospun membrane performance was achieved by employing BBD and the polynomial quadratic equation describing  $J_v/J_s$  as a simultaneous function of Con ( $X_1$ ), F ( $X_2$ ), and CD ( $X_3$ ), introduced in Eq. 12. The analysis of variance (ANOVA) was carried out at 95% confidence level to justify the significance and adequacy of the model and the p-value was used to determine the statistical significance of the factors or their combinations (Table 3). Therefore, an independent variable or an interaction was determined to be significant if the p-value was less than 0.05 and would be considered as insignificant by p-value of greater than 0.1. Accordingly, considering the selected confidence level,  $X_1X_3$  (Con  $\times$  CD) interaction was found to be insignificant and when removed from the proposed RMS model, Eq. 12 was modified as following

$$Y = -30.33 + 1.13\text{Con} + 7.28F + 14.99\text{CD} + 0.18\text{Con} \times F - 1.92F \times \text{CD} - 0.02\text{Con}^2 - 4.10F^2 - 2.26\text{CD}^2 \quad (14)$$

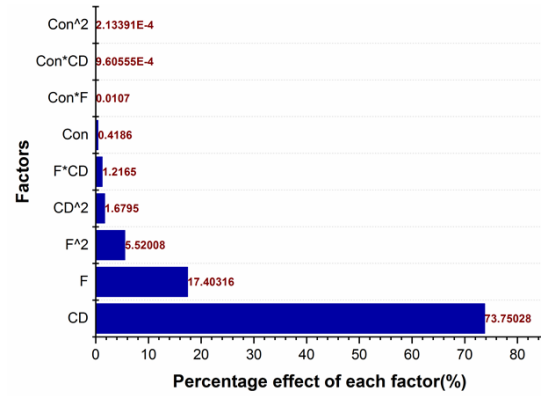


Fig. 3 Pareto chart representing the estimated impacts of parameters and parameter interactions on the model response ( $J_v/J_s$ ) (Eqs. 12 and 13)

Table 3 Analysis of variance (partial sum of squares)

Source	Sum of Squares	df	Mean Square	F Value	p-value Prob > F
Model	6.76	9	0.75	85.23	< 0.0001*
A-Con	0.78	1	0.78	88.02	< 0.0001
B-F	2.71	1	2.71	308.15	< 0.0001
C-CD	0.77	1	0.77	86.85	< 0.0001
AB	0.11	1	0.11	12	0.0134
AC	0.026	1	0.026	2.99	0.1344
BC	0.33	1	0.33	37.89	0.0008
A2	0.21	1	0.21	23.93	0.0027
B2	0.55	1	0.55	61.9	0.0002
C2	1.28	1	1.28	145.32	< 0.0001
Residual	0.053	6	8.81E-03		
Lack of Fit	0.034	3	0.011	1.76	0.3263**
Pure Error	0.019	3	6.38E-03		
Cor Total	6.81	15			

\* Significant

\*\* Not significant

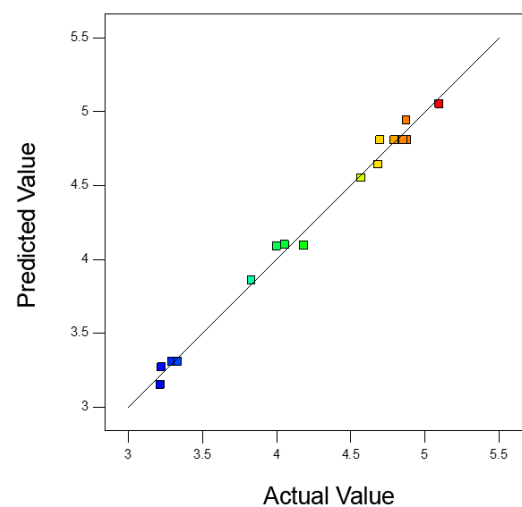


Fig. 4 Predicted values of model response versus the obtained experimental values

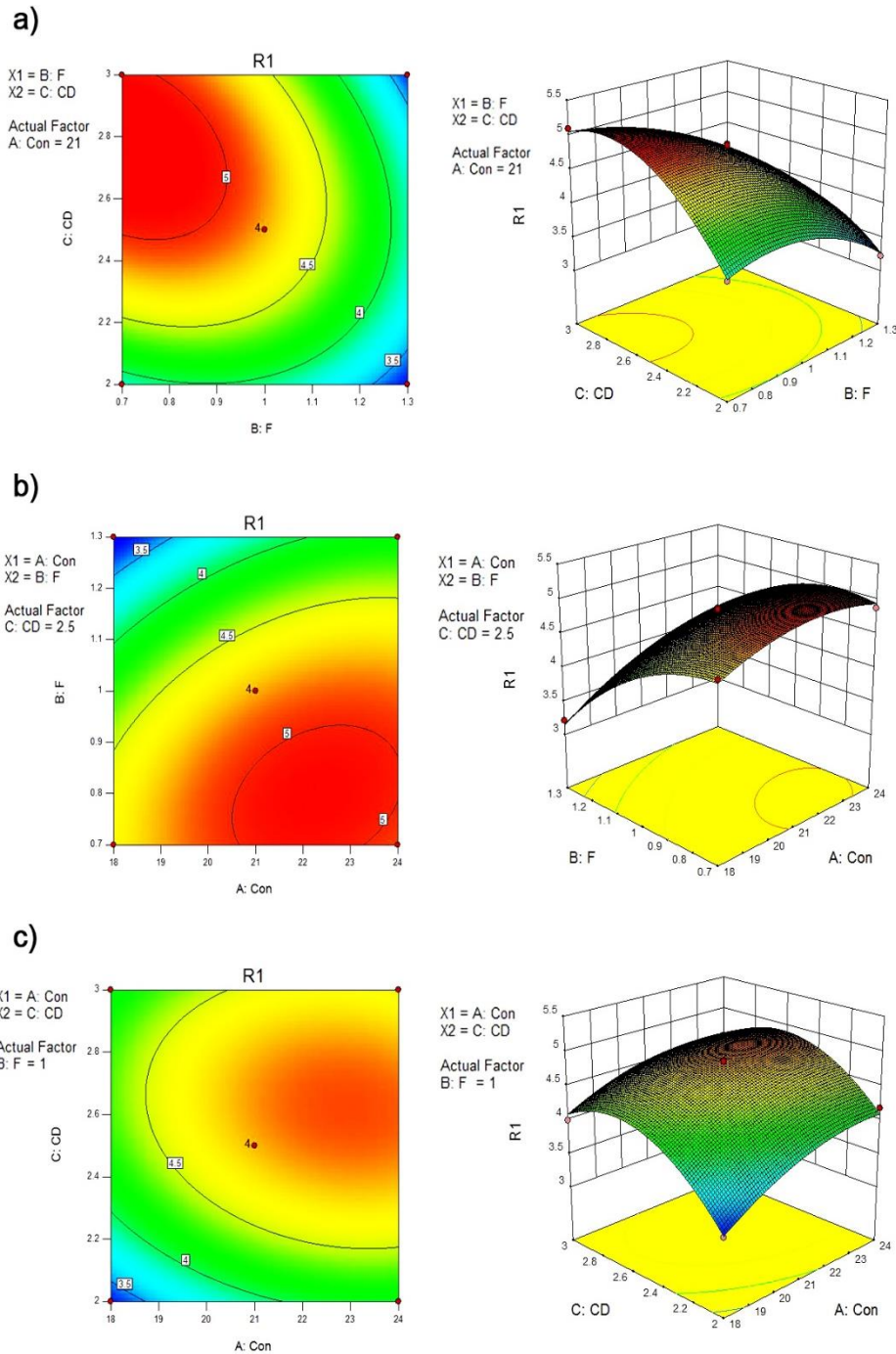


Fig. 5 Response surface showing interactions independent variable on the model response ( $J_v/J_s$ ). a) effects of CD and F, b) effects of F and Con, and c) effects of CD and Con

Table 4 Summary of the ANOVA results for the modified quadratic model

	Sequential	Lack of Fit	Adjusted	Predicted
Source	p-value	p-value	R-Squared	R-Squared
Linear	0.0067	0.0049	0.531	0.4037
2FI	0.592	0.0038	0.4887	0.2225
Quadratic	< 0.0001	0.3263	0.9806	0.9158
Cubic	0.3263		0.986	

■ Suggested  
□ Aliased

The above ultimate RSM models in terms of the coded factors were used to predict the experimental responses. All results were assessed with various descriptive statistics such p-value, F-value, degrees of freedom (df), determination coefficient ( $R^2$ ), adjusted  $R^2$ , sum of squares (SS), and mean sum of squares (MSS) to reflect the statistical significance of the developed quadratic model. Also, according to the obtained p-values (Table 4), the quadratic model was found to have the best fit to the data. The considerably low p-value (<0.0001) (Table 3) and relatively large absolute F-value (85.23) (Table 3), implied that the proposed model

Table 5 Obtained membrane characteristics and their FO performances

#	KW (LMH/bar)	R (%)	KS (LMH)	KS/KW (bar)	S ( $\mu\text{m}$ )	Thickness ( $\mu\text{m}$ )	Mean fiber diameter ( $\mu\text{m}$ )	Porosity (%)	Contact angle ( $^{\circ}$ )
1	4.51 $\pm$ 0.06	82.18 $\pm$ 0.11	0.2 $\pm$ 0.01	0.05 $\pm$ 0.01	686.53 $\pm$ 7.41	179.37 $\pm$ 4.91	2.57 $\pm$ 0.44	66.68 $\pm$ 7.13	135.30 $\pm$ 0.91
2	1.70 $\pm$ 0.03	91.03 $\pm$ 0.12	0.04 $\pm$ 0.01	0.02 $\pm$ 0.00	1369.68 $\pm$ 2.96	225.73 $\pm$ 7.01	3.88 $\pm$ 0.45	62.31 $\pm$ 1.33	134.48 $\pm$ 1.29
3	2.19 $\pm$ 0.01	87.7 $\pm$ 0.12	0.06 $\pm$ 0.01	0.03 $\pm$ 0.00	973.14 $\pm$ 1.48	221.53 $\pm$ 3.01	2.56 $\pm$ 0.81	78.55 $\pm$ 3.49	123.98 $\pm$ 1.36
4	4.03 $\pm$ 0.03	83.6 $\pm$ 0.12	0.17 $\pm$ 0.00	0.04 $\pm$ 0.00	703.53 $\pm$ 6.66	233.03 $\pm$ 2.76	2.18 $\pm$ 0.45	46.51 $\pm$ 2.48	126.65 $\pm$ 1.34
5	3.11 $\pm$ 0.08	84.8 $\pm$ 0.12	0.23 $\pm$ 0.01	0.05 $\pm$ 0.00	714.04 $\pm$ 6.88	368.10 $\pm$ 7.34	3.86 $\pm$ 0.57	72.63 $\pm$ 7.71	123.28 $\pm$ 0.28
6	1.63 $\pm$ 0.03	92.31 $\pm$ 0.13	0.03 $\pm$ 0.00	0.02 $\pm$ 0.00	1422.87 $\pm$ 1.72	219.80 $\pm$ 5.30	2.35 $\pm$ 0.45	86.92 $\pm$ 3.22	123.89 $\pm$ 0.89
7	1.21 $\pm$ 0.01	95.28 $\pm$ 0.12	0.01 $\pm$ 0.00	0.01 $\pm$ 0.00	1909.8 $\pm$ 6.12	199.97 $\pm$ 5.05	2.77 $\pm$ 0.47	76.55 $\pm$ 1.83	136.02 $\pm$ 1.28
8	2.25 $\pm$ 0.03	87.09 $\pm$ 0.12	0.07 $\pm$ 0.00	0.03 $\pm$ 0.00	917.14 $\pm$ 2.18	203.50 $\pm$ 8.05	3.08 $\pm$ 0.57	80.28 $\pm$ 2.92	127.26 $\pm$ 0.96
9	3.10 $\pm$ 0.02	84.95 $\pm$ 0.12	0.12 $\pm$ 0.00	0.04 $\pm$ 0.00	739.89 $\pm$ 1.76	177.35 $\pm$ 4.86	2.69 $\pm$ 0.4	66.38 $\pm$ 7.06	135.56 $\pm$ 0.94
10	1.30 $\pm$ 0.06	94.22 $\pm$ 0.11	0.02 $\pm$ 0.00	0.02 $\pm$ 0.01	1825.14 $\pm$ 1.72	204.00 $\pm$ 7.94	2.19 $\pm$ 0.37	66.25 $\pm$ 6.77	125.76 $\pm$ 0.72
11	2.49 $\pm$ 0.08	86.53 $\pm$ 0.12	0.08 $\pm$ 0.00	0.03 $\pm$ 0.00	793.77 $\pm$ 2.94	210.03 $\pm$ 5.00	3.13 $\pm$ 0.5	82.24 $\pm$ 5.78	128.37 $\pm$ 0.59
12	4.57 $\pm$ 0.06	80.99 $\pm$ 0.12	0.23 $\pm$ 0.00	0.05 $\pm$ 0.00	671.46 $\pm$ 26.88	249.87 $\pm$ 5.01	2.37 $\pm$ 0.29	45.39 $\pm$ 2.24	129.47 $\pm$ 0.99
13	1.53 $\pm$ 0.03	93.29 $\pm$ 0.12	0.02 $\pm$ 0.00	0.01 $\pm$ 0.00	1655.66 $\pm$ 3.50	318.27 $\pm$ 4.83	2.85 $\pm$ 0.56	58.86 $\pm$ 4.82	122.59 $\pm$ 1.12
14	3.08 $\pm$ 0.02	85.33 $\pm$ 0.10	0.11 $\pm$ 0.00	0.04 $\pm$ 0.00	761.56 $\pm$ 4.84	178.22 $\pm$ 4.84	2.48 $\pm$ 0.33	65.94 $\pm$ 6.94	135.86 $\pm$ 0.95
15	3.04 $\pm$ 0.01	85.48 $\pm$ 0.11	0.11 $\pm$ 0.00	0.04 $\pm$ 0.00	773.89 $\pm$ 2.99	179.00 $\pm$ 4.42	2.37 $\pm$ 0.32	66.04 $\pm$ 5.95	136.00 $\pm$ 0.91
16	2.75 $\pm$ 0.08	86.09 $\pm$ 0.12	0.12 $\pm$ 0.01	0.04 $\pm$ 0.01	777.19 $\pm$ 2.64	303.03 $\pm$ 7.13	3.96 $\pm$ 0.46	34.18 $\pm$ 4.25	122.78 $\pm$ 1.03
OPT	4.58 $\pm$ 0.03	80.11 $\pm$ 0.11	0.24 $\pm$ 0.00	0.05 $\pm$ 0.00	625.46 $\pm$ 4.97	183.33 $\pm$ 7.64	2.27 $\pm$ 0.33	61.96 $\pm$ 0.016	130.27 $\pm$ 0.80

was significant. The determination coefficient ( $R^2$ ) indicates to what extent the variability in the response values can be justified by the selected model variables.

Thus, the determination coefficient of 0.9158 calculated through ANOVA (Table 4) indicated that only 8.42 % of the total variations could not be explained by the quadratic regression model. Additionally, the value of the adjusted determination coefficient revealed that more than 98% of variations of the dependent variable could be anticipated by the model independent variables, thereby, as opposed to the  $R^2$  value, the model was confirmed to be highly significant. Moreover, the Lack of Fit F-value of 1.76 implied that the lack of fit was not significant when compared to the pure error and there was 32.63% chance that such a Lack of Fit F-value be due to noise.

Therefore, it could be concluded that the non-significant lack of fit was considered good and was desired for the model to fit, meaning that in the developed model, all the proposed variables were significant (M.Mourabet *et al.* 2014; Shanmugaparakash and Sivakumar, 2013; Vatanpour *et al.* 2017). Furthermore, the similarity between predicted (Eq. 14) and actual results obtained experimentally confirmed the accuracy and applicability of the Box–Behnken model as a powerful method for process optimization.

### 3.2.2 3D response surface with contour plot

Using Eq. 12, 3D response surface plots were developed for  $J_v/J_s$  (Figs. 5) in which the  $J_v/J_s$  were plotted against two independent variables while the third was held at its respective center values to depict the interactive effects of independent variables on responses. The nature and the extent of the interactions between different variables could

be inferred by the shapes of response surfaces and corresponding contour plots. The results revealed that the variables of interest (i.e. polymer concentration, flowrate and current density) were able to substantially affect the response in this study. The optimal values of the variables calculated in coded units and converted to real measure response values have been shown in Table 2. In addition, low impact of the interaction between CD and Con could also be verified in 3D plots, which was in line with the reported p-values of Table 3.

Characteristics of the FO membranes assessed for all membranes fabricated based on the experimental design Table 5, the lower the values of  $K_s$  and  $S$ , the better the (Table 2) have been summarized in Table 5. As shown, among all the fabricated FO membranes, the lowest  $S$  value was obtained in RUN 12. This was in accordance with the results obtained for the membrane performances in which the highest  $J_v/J_s$  was achieved for the same membrane. In performance of the membrane would be, whereas the high concentration values correspond to less efficient membranes. In Table 5, the lower the values of  $K_s$  and  $S$ , the better the performance of the membrane would be, whereas the high concentration values correspond to less efficient membranes. The characteristics of the electrospun membranes indicated that, in line with the results obtained through Pareto chart, CD and F parameters could be controlled to significantly influence the membrane characteristics and be manipulated to achieve the membranes of the best FO performances with the highest water fluxes. In such membranes, the  $S$  value would also be minimal, leading to reduced ICP and fouling propensity. By using the water fluxes determined in FO mode (Eqs. 7 and 9), following equation was employed to calculate the

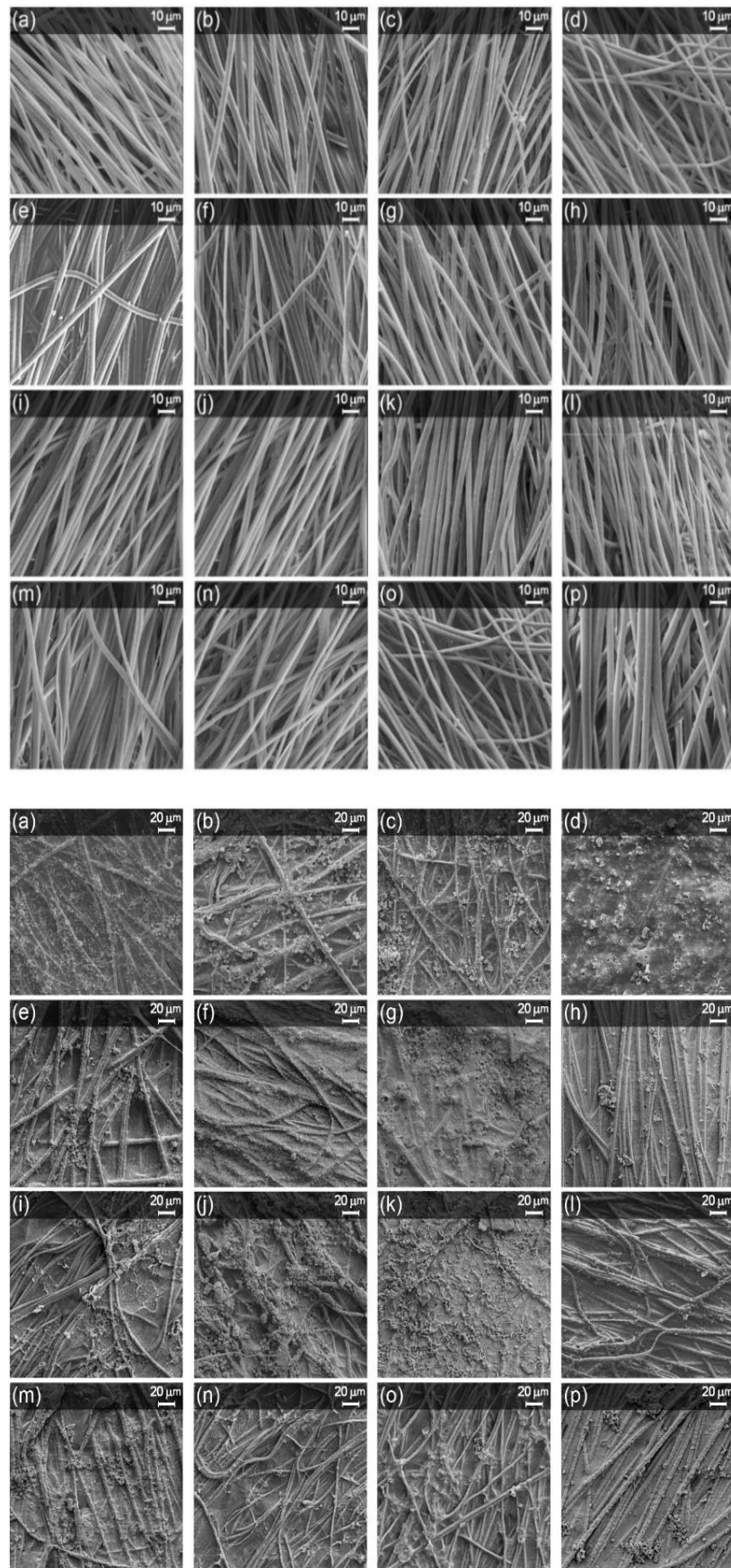


Fig. 6 A) SEM images of electrospun PSU membranes (support layers) from different PSU concentrations, flow rate, and current density for Run 1 to 16 denoted as (a) to (p), respectively. B) SEM images of electrospun PSU/polyamide (active layers) from different PSU concentrations, flowrate, and current density for Run 1 to 16 denoted as (a) to (p), respectively

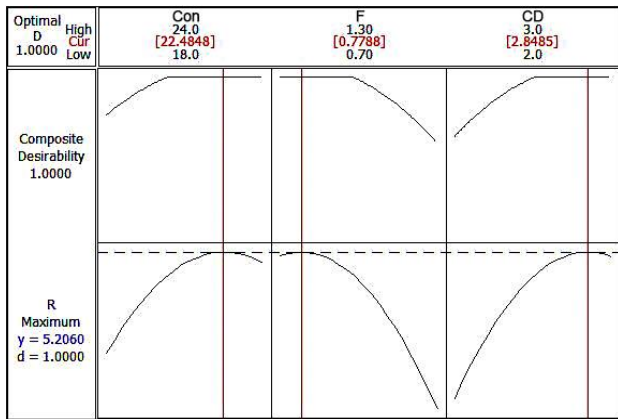


Fig. 7 The values of optimum point response and desirability

effective S value of the membrane

$$S = \frac{D_s}{J_v} \ln \frac{K_S + K_W \pi_{D,b}}{K_S + J_v + K_W \pi_{F,m}} \quad (15)$$

The obtained results revealed that, in FO mode of operation, increased CD and reduced F values could result in lower S parameter. However, similar to that reported in Pareto chart, the CD had more severe influence on the S parameter and overall membrane performance. Also, high CD and low F values would lead to the formation of narrow nanofibers that could in turn result in reduced membrane porosity and consequently membranes of reduced S parameter.

### 3.3 Membranes morphologies

Scanning electron microscope was used to study the morphology of the electrospun PSU fibers. Fig.6 shows the SEM images obtained from the ESPSU and TFCPSU. Based on the performed experimental design, each membrane was prepared under different operational conditions (Table 2).

As shown in the obtained images, reduced diameters of the randomly aligned nanofibers could be explained by the low flowrates used to inject the polymers and the short distance between the needle tip and the collector (fixed at 10 cm). It could also be inferred that, combination of the Con of 21%, reduced F, and high CD (RUN 12) could result in minimal S value as shown in Table 5. Additionally, F and CD were found to have the greatest influences on the structure of the obtained nanofibers.

### 3.4 Optimization studies

As shown in Fig. 7, the optimum values of Con, Cd, and F resulting in maximum response of 5.2 L/g and minimum S parameter were predicted by the Design Expert to be 22.48 %, 2.85 kV/cm, and 0.78 mL/hr, respectively. At the optimum point, Jv was determined to be 158.57 LMH and 46.88 in PRO mode and FO mode, respectively. Also, the observed response of Jv/Js was found to be 5.1630 L/gr, while the value predicted by the developed model was 5.2060 L/gr, implying the accuracy of the developed model.

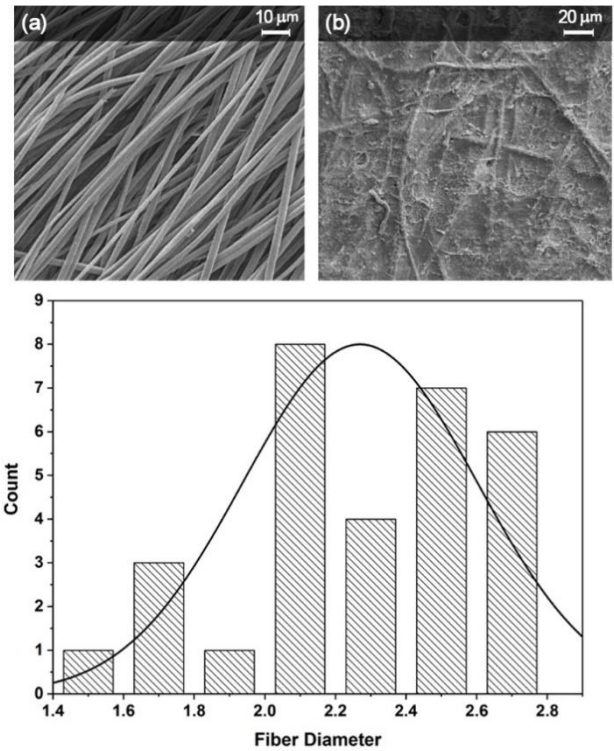


Fig. 8 SEM image of (a) support layer (PSU), and (b) active layer (PSU/polyamide) and its corresponding fiber diameter at optimum point. (c) Mean fiber diameter was determined to be  $2.27 \pm 0.33 \mu\text{m}$  which was consistent with the values reported in Table 5

Table 6 Comparing the best experiment and the optimal point in terms of having the minimum value of the S value

RUN #	CD (kV/cm)	F (ml/hr)	Con (%)	S ( $\mu\text{m}$ )
12	3	0.7	21	$671.46 \pm 26.88$
OPT Point	2.8	0.8	22.48	$625.46 \pm 4.97$

To better study the morphology of the membrane of the best performance which was fabricated using the optimum values, SEM images were provided used to determine its fiber diameter distribution (Fig. 8).

According to the results summarized in Table 5, the highest response was achieved in RUN 12, which was also found to possess the lowest S value. Accordingly, as expected, the optimal values obtained for the 3 influencing parameters in this study were practically similar to that of RUN 12 in which the highest response and the lowest S values were achieved (Table 6). This implied the accuracy and precision of the conducted experimental procedures as well as the optimization strategy used in this study to verify the best parameters that could lead to the membrane of the best performance.

## 4. Conclusions

Based on Box–Behnken design, performance of electrospun membrane was optimized through minimization of membrane structural parameter using response surface

methodology. Three independent influencing parameters of the electrospinning process that were determined to have the highest impact on the performance of the fabricated membrane, including the flowrate (F), polymer concentration (Con), and current density (CD) were optimized to minimize the structural parameter of the electrospun membrane. Based on the statistical analyses, current density was found to have the highest effect on the membrane performance in terms of the water flux to reverse salt flux ratio and flowrate revealed the less impact. The obtained results revealed that decreased flowrate besides increased current density and polymer concentration had positive impact on overall membrane performance. Additionally, quadratic terms of  $CD^2$  and  $F^2$  as well as the interaction term of  $F \times CD$  were found to be significant in electrospinning process. The high determination coefficient and adjusted determination coefficient found via the analysis of variance also indicated that the regression model that was developed via Box–Behnken design was in good agreement with the experimental data. Furthermore, by conducting optimization analysis, the optimal values of CD, Con, and F were determined to be 22.48 %, 2.8 kV/cm, and 0.8 mL/min, respectively. The adequacy check of the model also revealed that the developed quadratic model was satisfactory and accurate with no significant differences between observed and predicted results, implying that the obtained results can be considered to better understand the factors influencing the electrospun membrane characteristics and can be used in electrospinning processes to manipulate electrospun membrane characteristics and achieve electrospun membranes of high performance and improved efficiency.

## Acknowledgements

The authors gratefully acknowledge the instrumental supports received by University of Tehran. Also, high pure NaCl salt received by the Iran Mineral Salts Company is appreciated.

## References

- Alsvik, I.L. and Hägg, M.B. (2013), “Pressure retarded osmosis and forward osmosis membranes: Materials and methods”, *Polymers (Basel)*, **5**, 303–327. <https://doi.org/10.3390/polym5010303>
- Altaee, A. and Sharif, A. (2015), “Pressure retarded osmosis: advancement in the process applications for power generation and desalination”, *Desalination*, **356**, 31–46. <https://doi.org/10.1016/j.desal.2014.09.028>
- Barhate, R.S., Loong, C.K. and Ramakrishna, S. (2006), “Preparation and characterization of nanofibrous filtering media”, *J. Memb. Sci.*, **283**, 209–218. <https://doi.org/10.1016/J.MEMSCI.2006.06.030>
- Bjorge, D., Daels, N., De Vrieze, S., Dejans, P., Van Camp, T., Audenaert, W., Hogue, J., Westbroeck, P., De Clerck, K. and Van Hulle, S.W.H. (2009), “Performance assessment of electrospun nanofibers for filter applications”, *Desalination*, **249**, 942–948. <https://doi.org/10.1016/J.DESAL.2009.06.064>
- Bui, Nhu-ngoc and McCutcheon, R. (2013), “Hydrophilic Nano fibers as New Supports for Thin Film Composite Membranes for Engineered Osmosis”, *Environ. Sci. Technol.*, **47**, 1761–1769. <https://doi.org/10.1021/es304215g>
- Bui, N., Laura, M., Hoek, E.M.V. and McCutcheon, J.R. (2011), “Electrospun nanofiber supported thin film composite membranes for engineered osmosis”, *J. Memb. Sci.*, **385**–386, 10–19. <https://doi.org/10.1016/j.memsci.2011.08.002>
- Bui, N.N., McCutcheon, J.R. (2014), “Nanofiber supported thin-film composite membrane for pressure-retarded osmosis”, *Environ. Sci. Technol.*, **48**, 4129–4136. <https://doi.org/10.1021/es4037012>
- Cojocaru, C., Pascariu, P., Airinei, A., Olaru, N., Samoila, P., Rotaru, A. (2017), “Design and evaluation of electrospun polysulfone fibers and polysulfone /NiFe<sub>2</sub>O<sub>4</sub> nanostructured composite as sorbents for oil spill cleanup”, *J. Taiwan Inst. Chem. Eng.*, **70**, 267–281. <https://doi.org/10.1016/j.jtice.2016.11.005>
- Ferreira, S.L.C., Bruns, R.E., Ferreira, H.S., Matos, G.D., David, J.M., Brandão, G.C., da Silva, E.G.P., Portugal, L.A., dos Reis, P.S., Souza, A.S. and dos Santos, W.N.L. (2007), “Box-Behnken design: An alternative for the optimization of analytical methods”, *Anal. Chim. Acta*, **597**, 179–186. <https://doi.org/10.1016/j.aca.2007.07.011>
- Ge, Q., Ling, M. and Chung, T. (2013), “Draw solutions for forward osmosis processes: Developments, challenges and prospects for the future”, *J. Memb. Sci.* **442**, 225–237. <https://doi.org/10.1016/j.memsci.2013.03.046>
- Gönen, S.Ö., Erol Taygun, M. and Küçükbayrak, S. (2016), “Evaluation of the factors influencing the resultant diameter of the electrospun gelatin/sodium alginate nanofibers via Box-Behnken design”, *Mater. Sci. Eng. C*, **58**, 709–723. <https://doi.org/10.1016/j.msec.2015.09.024>
- Hoover, L.A., Schiffman, J.D. and Elimelech, M. (2013), “Nanofibers in thin-film composite membrane support layers: Enabling expanded application of forward and pressure retarded osmosis”, *Desalination*, **308**, 73–81. <https://doi.org/10.1016/J.DESAL.2012.07.019>
- Huang, L., Bui, N., Meyering, M.T., Hamlin, T.J. and McCutcheon, J.R. (2013), “Novel hydrophilic nylon 6, 6 microfiltration membrane supported thin film composite membranes for engineered osmosis”, *J. Memb. Sci.*, **437**, 141–149. <https://doi.org/10.1016/j.memsci.2013.01.046>
- Khataee, A.R., Zarei, M. and Moradkhannejhad, L. (2010), “Application of response surface methodology for optimization of azo dye removal by oxalate catalyzed photoelectro-Fenton process using carbon nanotube-PTFE cathode”, *Desalination*, **258**, 112–119. <https://doi.org/10.1016/j.desal.2010.03.028>
- Kim, D.Y., Oh, Y.K., Park, J.Y., Kim, B., Choi, S.A. and Han, J.I. (2015), “An integrated process for microalgae harvesting and cell disruption by the use of ferric ions”, *Bioresour. Technol.*, **191**, 469–474. <https://doi.org/10.1016/j.biortech.2015.03.020>
- Klaysom, C., Cath, T.Y., Depuydt, T. and Vankelecom, I.F.J. (2013), “Forward and pressure retarded osmosis: potential solutions for global challenges in energy and water supply”, *Chem. Soc. Rev.*, **42**, 6959. <https://doi.org/10.1039/c3cs60051c>
- Li, G., Li, P., Yu, Y., Jia, X., Zhang, S., Yang, X. and Ryu, S. (2008), “Novel carbon fiber / epoxy composite toughened by electrospun polysulfone nanofibers”, **62**, 511–514. <https://doi.org/10.1016/j.matlet.2007.05.080>
- Li, W., Gao, Y. and Tang, C.Y. (2011), “Network modeling for studying the effect of support structure on internal concentration polarization during forward osmosis: Model development and theoretical analysis with FEM”, *J. Memb. Sci.*, **379**, 307–321. <https://doi.org/10.1016/j.memsci.2011.05.074>
- Liu, Q., Li, J., Zhou, Z., Qiu, G., Xie, J. and Lee, J.Y. (2016), “Dual-Functional Coating of Forward Osmosis Membranes for Hydrophilization and Antimicrobial Resistance”, *Adv. Mater. Interfaces*, **3**, 1–8. <https://doi.org/10.1002/admi.201500599>

- Liu, Q., Zhou, Z., Qiu, G., Li, J., Xie, J. and Lee, J.Y. (2015), "Surface Reaction Route To Increase the Loading of Antimicrobial Ag Nanoparticles in Forward Osmosis Membranes", *ACS Sustain. Chem. Eng.*, **3**, 2959–2966. <https://doi.org/10.1021/acssuschemeng.5b00931>.
- Liu, X. and Ng, H.Y. (2015), "Fabrication of layered silica-polysulfone mixed matrix substrate membrane for enhancing performance of thin-film composite forward osmosis membrane", *J. Memb. Sci.*, **481**, 148–163. <https://doi.org/10.1016/j.memsci.2015.02.012>
- Loeb, S., Titelman, L., Korngold, E. and Freiman, J. (1997), "Effect of porous support fabric on osmosis through a Loeb-Sourirajan type asymmetric membrane", *J. Memb. Sci.*, **129**, 243–249. [https://doi.org/10.1016/S0376-7388\(96\)00354-7](https://doi.org/10.1016/S0376-7388(96)00354-7)
- Lutchmiah, K., Verliefe, A.R.D., Roest, K. and Rietveld, L.C. (2014), "ScienceDirect Forward osmosis for application in wastewater treatment: A review", *Water Res.*, **58**, 179–197. <https://doi.org/10.1016/j.watres.2014.03.045>
- Mourabet, M., El Rhilassi, A., Bennani-Ziatni, M. and Taitai, A. (2014), "Comparative Study of Artificial Neural Network and Response Surface Methodology for Modelling and Optimization the Adsorption Capacity of Fluoride onto Apatitic Tricalcium Phosphate", *Univers. J. Appl. Math.*, **2**, 84–91. <https://doi.org/10.13189/ujam.2014.020202>
- McCutcheon, J.R. and Elimelech, M. (2008), "Influence of membrane support layer hydrophobicity on water flux in osmotically driven membrane processes", *J. Memb. Sci.*, **318**, 458–466. <https://doi.org/10.1016/j.memsci.2008.03.021>
- McCutcheon, J.R. and Elimelech, M. (2006), "Influence of concentrative and dilutive internal concentration polarization on flux behavior in forward osmosis", *J. Memb. Sci.*, **284**, 237–247. <https://doi.org/10.1016/j.memsci.2006.07.049>
- Montgomery, M.A. and Elimelech, M. (2007), "Water and sanitation in developing countries: Including health in the equation - Millions suffer from preventable illnesses and die every year", *Environ. Sci. Technol.*, **41**, 17–24. <https://doi.org/10.1021/es072435t>
- Muscattello, J., Müller, E.A., Mostofi, A.A. and Sutton, A.P. (2017), "Multiscale molecular simulations of the formation and structure of polyamide membranes created by interfacial polymerization", *J. Memb. Sci.*, **527**, 180–190. <https://doi.org/10.1016/j.memsci.2016.11.024>
- Nam, S.N., Cho, H., Han, J., Her, N. and Yoon, J. (2018), "Photocatalytic degradation of acetylacetone K: Optimization using the Box–Behnken design (BBD)", *Process Saf. Environ. Prot.*, **113**, 10–21. <https://doi.org/10.1016/j.psep.2017.09.002>
- Obaid, M., Ghouri, Z.K., Fadali, O.A., Khalil, K.A., Almajid, A.A. and Barakat, N.A.M. (2016a), "Amorphous SiO<sub>2</sub> NP-Incorporated Poly(vinylidene fluoride) Electrospun Nanofiber Membrane for High Flux Forward Osmosis Desalination", *ACS Appl. Mater. Interfaces*, **8**, 4561–4574. <https://doi.org/10.1021/acsami.5b09945>
- Obaid, M., Mohamed, H.O., Yasin, A.S., Fadali, O.A., Khalil, K.A., Kim, T. and Barakat, N.A.M. (2016b), "A novel strategy for enhancing the electrospun PVDF support layer of thin-film composite forward osmosis membranes", *RSC Adv.* **6**, 102762–102772. <https://doi.org/10.1039/C6RA18153H>
- Park, M.J., Gonzales, R.R., Abdel-Wahab, A., Phuntsho, S. and Shon, H.K. (2018), "Hydrophilic polyvinyl alcohol coating on hydrophobic electrospun nanofiber membrane for high performance thin film composite forward osmosis membrane", *Desalination*, **426**, 50–59. <https://doi.org/10.1016/j.desal.2017.10.042>
- Pascariu-dorneanu, P., Airinei, A., Oлару, N., Fifere, N., Doroftei, C. and Iacomi, F. (2017), "Preparation and characterization of some electrospun polysulfone nanocomposites reinforced with Ni doped SnO<sub>2</sub> nanoparticles", *Eur. Polym. J.*, **91**, 326–336. <https://doi.org/10.1016/j.eurpolymj.2017.04.004>
- Rastgar, M., Bozorg, A. and Shakeri, A. (2018), "Novel Dimensionally Controlled Nanopore Forming Template in Forward Osmosis Membranes", *Environ. Sci. Technol.* **52**, 7605–7612. <https://doi.org/10.1021/acs.est.7b05583>
- Rastgar, M., Shakeri, A., Bozorg, A., Salehi, H. and Saadattalab, V. (2017), "Impact of nanoparticles surface characteristics on pore structure and performance of forward osmosis membranes", *Desalination*, **420**, 1–11. <https://doi.org/10.1016/j.desal.2017.01.040>
- Salehi, H., Rastgar, M. and Shakeri, A. (2017a), "Anti-Fouling and High Water Permeable Forward Osmosis Membrane Fabricated via Layer by Layer Assembly of Chitosan / Graphene Oxide", *Appl. Surf. Sci.* **367**, 271–280. <https://doi.org/10.1016/j.apsusc.2017.03.271>
- Salehi, H., Shakeri, A. and Rastgar, M. (2017b), "Carboxylic polyethersulfone: A novel pH-responsive modifier in support layer of forward osmosis membrane", *J. Memb. Sci.*, **527**, 180–190. <https://doi.org/10.1016/j.memsci.2017.10.044>
- Shanmugaprakash, M. and Sivakumar, V. (2013), "Development of experimental design approach and ANN-based models for determination of Cr(VI) ions uptake rate from aqueous solution onto the solid biodiesel waste residue", *Bioresour. Technol.*, **148**, 550–559. <https://doi.org/10.1016/j.biortech.2013.08.149>
- Shannon, M., Bohn, P.W., Elimelech, M., Georgiadis, J.G., Mariñas, B.J. and Mayes, A.M. (2008), "Science and technology for water purification in the coming decades", *Nature*, **452**, 301–310. <https://doi.org/10.1038/nature06599>
- She, Q., Wang, R., Fane, A.G. and Tang, C.Y. (2016), "Membrane fouling in osmotically driven membrane processes: A review". *J. Memb. Sci.*, **499**, 201–233. <https://doi.org/10.1016/j.memsci.2015.10.040>
- Song, X., Liu, Z. and Sun, D.D. (2011), "Nano gives the answer: Breaking the bottleneck of internal concentration polarization with a nanofiber composite forward osmosis membrane for a high water production rate", *Adv. Mater.*, **23**, 3256–3260. <https://doi.org/10.1002/adma.201100510>
- Sudeeptha, G. and Arun Kumar Thalla. (2017), "Ranking and comparison of draw solutes in a forward osmosis process", *Membr. Water Treat.*, **8**, 411–421. <https://doi.org/10.12989/mwt.2017.8.5.411>
- Tiraferri, A., Yip, N.Y., Phillip, W.A., Schiffman, J.D. and Elimelech, M. (2011), "Relating performance of thin-film composite forward osmosis membranes to support layer formation and structure". *J. Memb. Sci.*, **367**, 340–352. <https://doi.org/10.1016/j.memsci.2010.11.014>
- Vatanpour, V., Sheydaei, M. and Esmaeili, M. (2017a), "Box-Behnken design as a systematic approach to inspect correlation between synthesis conditions and desalination performance of TFC RO membranes", *Desalination*, **420**, 1–11. <https://doi.org/10.1016/j.desal.2017.06.022>
- Vatanpour, V., Sheydaei, M. and Esmaeili, M. (2017b), "Box-Behnken design as a systematic approach to inspect correlation between synthesis conditions and desalination performance of TFC RO membranes", *Desalination*, **420**, 1–11. <https://doi.org/10.1016/j.desal.2017.06.022>
- Wang, R., Liu, Y., Li, B., Hsiao, B.S. and Chu, B. (2012), "Electrospun nanofibrous membranes for high flux microfiltration", *J. Memb. Sci.*, **392–393**, 167–174. <https://doi.org/10.1016/j.memsci.2011.12.019>
- Wang, R., Shi, L., Tang, C.Y., Chou, S., Qiu, C. and Fane, A.G. (2010), "Characterization of novel forward osmosis hollow fiber membranes", *J. Memb. Sci.*, **355**, 158–167. <https://doi.org/10.1016/j.memsci.2010.03.017>
- Wendorff, J.H., Agarwal, S. and Greiner, A. (2012), *Electrospinning: Materials, Processing, and Applications*, Wiley-VCH Verlag GmbH & Co. KGaA, Weinheim, Germany. <https://doi.org/10.1002/9783527647705>

- Werber, J.R., Osuji, C.O. and Elimelech, M. (2016), "Materials for next-generation desalination and water purification membranes", *Nat. Rev. Mater.*, **1**, 16018. <https://doi.org/10.1038/natrevmats.2016.18>.
- Wong, M.C.Y., Martinez, K., Ramon, G.Z. and Hoek, E.M.V. (2012), "Impacts of operating conditions and solution chemistry on osmotic membrane structure and performance", *Desalination*, **287**, 340–349. <https://doi.org/10.1016/j.desal.2011.10.013>.
- Xu, Y., Peng, X., Tang, C.Y., Fu, Q.S. and Nie, S. (2010), "Effect of draw solution concentration and operating conditions on forward osmosis and pressure retarded osmosis performance in a spiral wound module", *J. Memb. Sci.*, **348**, 298–309. <https://doi.org/10.1016/j.memsci.2009.11.013>.
- Yoon, K., Hsiao, B.S. and Chu, B. (2009), "High flux ultrafiltration nanofibrous membranes based on polyacrylonitrile electrospun scaffolds and crosslinked polyvinyl alcohol coating", *J. Memb. Sci.*, **338**, 145–152. <https://doi.org/10.1016/j.memsci.2009.04.020>.

CC